



ELSEVIER

Contents lists available at ScienceDirect

## Aerospace Science and Technology

journal homepage: [www.elsevier.com/locate/aescte](http://www.elsevier.com/locate/aescte)

# Sparse online Gaussian process adaptation for incremental backstepping flight control

Dmitry I. Ignatyev<sup>\*</sup>, Hyo-Sang Shin, Antonios Tsourdos

School of Aerospace, Transport and Manufacturing, Cranfield University, Cranfield MK43 0AL, UK

## ARTICLE INFO

### Article history:

Received 6 September 2022

Received in revised form 5 January 2023

Accepted 25 January 2023

Available online 31 January 2023

Communicated by Chaoyong Li

### Keywords:

Gaussian processes

Adaptive control

Parameter estimation

Incremental backstepping

Failures

Fault-tolerant control

## ABSTRACT

Presence of uncertainties caused by unforeseen malfunctions in actuation or measurement systems or changes in aircraft behaviour could lead to aircraft loss-of-control during flight. This paper considers sparse online Gaussian Processes (GP) adaptive augmentation for Incremental Backstepping (IBKS) flight control. IBKS uses angular accelerations and control deflections to reduce the dependency on the aircraft model. However, it requires knowledge of the relationship between inner and outer loops and control effectiveness. Proposed indirect adaptation significantly reduces model dependency. Global uniform ultimate boundness is proved for the resultant GP adaptive IBKS. Conducted research shows that if the input-affine property is violated, e.g., in severe conditions with a combination of multiple failures, the IBKS can lose stability. Meanwhile, the proposed sparse GP-based estimator provides fast online identification and the resultant controller demonstrates improved stability and tracking performance.

© 2023 The Authors. Published by Elsevier Masson SAS. This is an open access article under the CC BY license (<http://creativecommons.org/licenses/by/4.0/>).

## 1. Introduction

During the last decades, aircraft safety has significantly increased. Nevertheless, flight safety in abnormal conditions, such as those caused by equipment failures and/or adverse environmental factors, is still a challenging problem. Analysis of accident and incidence reports revealed that the main contribution to fatal accidents in passenger aviation was due to aircraft *loss of control in-flight* and *controlled flight into terrain* [1]. The main reasons caused these accidents are pilot mistakes, technical malfunctions, or their combination.

Recently, significant efforts have been undertaken to develop aircraft control design tools to improve flight safety [2–8]. The idea that non-conventional control strategies can prevent possible accidents and recover aircraft from dangerous situations stimulates research toward fault-tolerant and adaptive flight control [9–12].

Gain-scheduling of linear feedback controllers is widely applied in commercial applications to achieve stabilization and satisfactory tracking performance of aircraft over a wide range of flight conditions [13], [14]. In case of severe and unpredicted changes in aircraft behaviour, such controllers cannot be used or can be used only with restricted functionality.

Nonlinear Dynamics Inversion (NDI) and Backstepping (BS) techniques have become popular control strategies for adaptation since they can be used for global linearization of the system dynamics and control decoupling [15–20]. Later, an incremental-type sensor-based form was proposed to make NDI and BS controls more robust and fault-tolerant [21–23].

However, even in this formulation, the controller still requires accurate knowledge of the functional relationship between inner and outer loops and control effectiveness. For example, if the system is not affine in control inputs because of non-linearity in actuators or large transport delays, it may cause significant control degradation [24–26]. Adaptation strategies augmenting the incremental-type controllers were applied for a high-performance aircraft model in [25], [27] to reduce dependency on an aircraft model. Regardless of the fact that IBKS demonstrates robustness to some failures [28], [29] estimation of the control effectiveness improves the fault-tolerant abilities of the system [24], [30–33].

The most well-known and popular approach for on-line identification and implementation of in-direct adaptation is Recursive Least Squares (RLS) method [24], [27], [34], [35]. However, even with the conventional Exponential Forgetting factor (EF), RLS is not designed for tracking time-varying systems. Its convergence might be slow if the EF is close to one, whereas the error is large if the EF is small. The Tuning Functions (TF) approach was proposed as a natural expansion of the adaptive capabilities provided by the backstepping paradigm into the identification of control efficiency

<sup>\*</sup> Corresponding author.

E-mail address: [d.ignatyev@cranfield.ac.uk](mailto:d.ignatyev@cranfield.ac.uk) (D.I. Ignatyev).

## Nomenclature

$\mathbf{B}_0$	control effectiveness matrix
$\mathbf{T}_\xi$	matrix representing kinematic relationship between angular rates and kinematic variables
$g_y$	y-axis component of the gravitational acceleration calculated in the wind reference frame
$p, q, r$	roll, pitch, and yaw rates
$\mathbf{u}$	vector of control effectors
$V_t$	true airspeed
$\alpha, \beta$	angles of attack and sideslip
$\delta$	aircraft control surface deflection
$\xi$	attitude state vector

$\phi, \theta$	roll and pitch angles
$\boldsymbol{\omega}$	rotational rate vector

### Aerodynamic derivative

$$C_{m\delta} \quad \frac{\partial C_m}{\partial \delta}$$

### Subscripts

d	desired value
y	variable related to dynamics
$\xi$	variable related to kinematics
$\omega$	variable related to angular rates

[16], [24], [27]. This approach takes advantage of the Lyapunov function design, which allows theoretical proof of stability. However, these methods can be sensitive to measurement noise. It should be also noted that the indirect adaptation methods require Persistency of Excitation (PE). Without PE, the parameter estimates might be incorrect, leading to incorrect control actions, sensitivities and system instabilities [36].

Neural networks, including Radial Basis Functions (RBF), are quite popular for online identification and adaptive control since they are universal approximators and can match any uncertainty (for example, see [37–39]). RBFs have the advantage, namely, they are linear-in-the-parameters, as opposed to multilayer perceptron neural networks. However, the performance of the former approach is significantly determined by a selection of the RBF centres. Normally, researchers preallocate a fixed quantity of Gaussian RBF centres over the presumed domain [37], [40]. The system states must stay close to the location of the preallocated RBF centres because a Gaussian RBF output decays exponentially away from its centre; otherwise, the system would not be able to capture the uncertainty.

To tackle the issues mentioned above, we propose to use a sparse Gaussian Process (GP) online identification framework to estimate control derivatives as well as the functional relationships between inner and outer control loops. In such a way, an in-direct adaptive control loop augmenting the baseline IBKS controller is implemented. GP brings promising Bayesian paradigm to online identification and adaptive control by considering the estimation as a statistical problem [41], [42]. Within the proposed approach GPs utilize a Bayesian framework to represent uncertainties as a distribution over functions. It is assumed that the uncertainty and the model follow Gaussian distributions, with the uncertainty being estimated using its mean and covariance function. One of the advantages of the proposed method is that it does not require prior assumptions about an operating domain. From the provided flight data, GP can dynamically choose new kernel locations to guarantee domain coverage. Furthermore, measurement noise is explicitly handled, and parameters such as the centres of RBFs do not require pre-allocation. GP approach allows Bayesian inference to overcome shortcomings of the standard gradient-based parameter update laws, e.g., lack of convergence guarantees and possible instabilities under noise presence [43], [44]. This method was applied for the design of direct adaptive control GP-MRAC in [45], [46], where GP was used to match an uncertainty to produce compensating control commands.

In the current paper, we developed a GP-based estimator of control efficiency and kinematic relationship to be fed into the baseline IBKS aircraft flight control system. The paper proposes a budgeted sparse GP algorithm suitable for on-line identification and adaptation. The framework proposes a model free control strategy guaranteeing stability even in case of actuator failures,

imprecise measurement and other uncertainties. The GP-based estimator provides fast convergence and long-term memory capabilities. Global uniform ultimate boundedness for the resultant GP adaptive IBKS is also considered in the paper. The performance of the method is demonstrated via simulations in three different scenarios, when uncertainties are introduced in the control efficiency. Comparative analysis manifests that the developed approach overperforms EF RLS and TF adaptations.

The present paper demonstrates results from the European project INCEPTION, which was seeking the development of a fault-tolerant Automatic Flight Control System for fixed-wing aircraft allying incremental control strategies, adaptive augmentation and envelope protection [47]. The proposed augmentation improves the stability and tracking performance of the IBKS baseline controller by providing actual information about control effectiveness in case of uncertainty or failure. According to the conventional approach for the validation of flight-critical systems [48], the performance of the augmented control system is evaluated through several worst-case scenarios.

The paper is organized in the following way. A very brief overview of the flight dynamics and IBKS control strategy are given in Sections 2 and 3 correspondingly. Section 4 describes the identification framework in general. The budgeted sparse GP algorithm is considered in Section 5. EF RLS and TF estimation algorithms are presented in Section 6. Section 7 provides and analyzes the simulation results of the proposed framework. Finally, concluding remarks are summarized in Section 8.

## 2. Flight dynamics model

Equations of angular motions of the aircraft can be represented with kinematics and dynamics models from [49]. The kinematics of the aircraft is described by the attitude state vector  $\xi = [\phi \ \theta \ \beta]^T$ .

$$\dot{\xi} = \mathbf{f}_\xi + \mathbf{T}_\xi \boldsymbol{\omega}, \quad (1)$$

where

$$\mathbf{f}_\xi = \begin{bmatrix} 0 & 0 & -\frac{A_x}{V_t} \cos \alpha \sin \beta + \frac{A_y}{V_t} \cos \beta - \frac{A_z}{V_t} \sin \alpha \sin \beta + \frac{g_y}{V_t} \end{bmatrix}^T,$$

$$\mathbf{T}_\xi = \begin{bmatrix} 1 & \sin \phi \tan \theta & \cos \phi \tan \theta \\ 0 & \cos \phi & -\sin \phi \\ \sin \alpha & 0 & -\cos \alpha \end{bmatrix}.$$

Specific forces  $A_x$ ,  $A_y$  and  $A_z$  can be directly measured by the accelerometers.

The aircraft dynamics is represented with the state-space form for the state vector  $\mathbf{y} = [V_t \ p \ q \ r]^T$  composed of airspeed  $V_t$ , roll rate  $p$ , pitch rate  $q$  and yaw rate  $r$ .

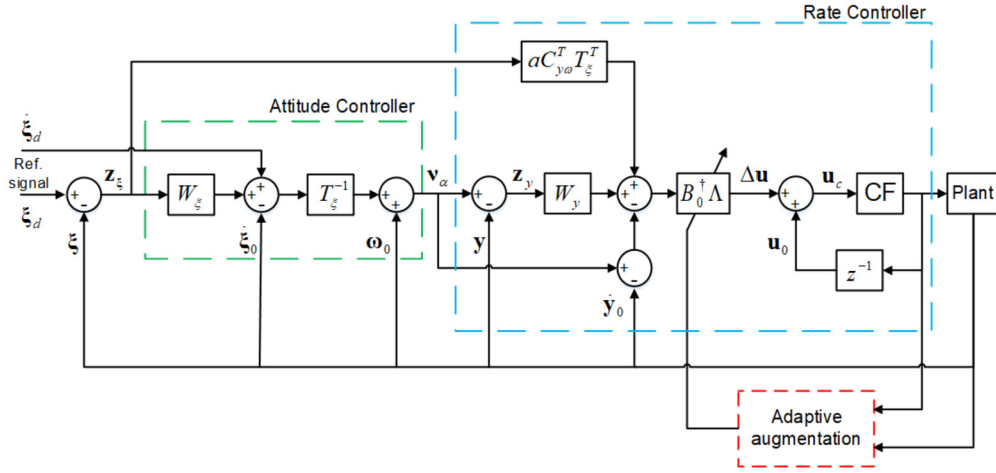


Fig. 1. Controller structure with control efficiency adaptation.

$$\dot{\mathbf{y}} = \mathbf{f}_y(\mathbf{y}, \mathbf{u}), \quad (2)$$

where  $\mathbf{u}$  is the control input vector.

Typically, the aircraft flight dynamics equations are typically assumed to have input-affine property, however, in this research, this assumption is relaxed, and the flight dynamics is considered in the generalised form of Eq. (2). In the further sections, Eq. (2) is simplified using the incremental dynamics approach for the incremental controller design in such a way that only control efficiency matrix is used. That is why the full aircraft nonlinear dynamics model  $\mathbf{f}_y(\mathbf{y}, \mathbf{u})$  is not provided here, however, it can be found in the literature (e.g. [35]).

### 3. Incremental backstepping

A sensor-based technique utilizing Incremental Dynamics (ID) applied to obtain an IBKS controller, which is less dependent on the system model, is discussed in [49], [50]. Below, we will just follow a brief description of this controller. The details could be found in the original papers. IBKS computes incremental commands employing acceleration feedback estimations to extract unmodeled flight dynamics. In the present study, we are using this controller as a baseline controller, which is augmented with the proposed budgeted sparse GP parameter estimator.

#### 3.1. Incremental dynamics model

It is assumed here that the system dynamics is described by the following nonlinear equations:

$$\dot{\mathbf{x}} = \mathbf{f}_x(\mathbf{x}, \mathbf{u}) \quad (3)$$

where  $\mathbf{f}_x: \mathbb{R}^n \times [0, \infty) \rightarrow \mathbb{R}^n$  is Lipschitz continuous function,  $\mathbf{x}$  and  $\mathbf{u}$  are the state and the control input vectors. To obtain an incremental form of system dynamics, we consider a first-order Taylor series expansion not in the geometric sense but with respect to a sufficiently small time delay [51]. Expanding (3) into the Taylor series around  $(\mathbf{x}_0, \mathbf{u}_0)$  corresponding to the previous time moment  $t_0$  the dynamics (3) can be expressed in the following form

$$\dot{\mathbf{x}} \cong \dot{\mathbf{x}}_0 + \frac{\partial \mathbf{f}_x(\mathbf{x}, \mathbf{u})}{\partial \mathbf{x}}(\mathbf{x} - \mathbf{x}_0) + \frac{\partial \mathbf{f}_x(\mathbf{x}, \mathbf{u})}{\partial \mathbf{u}}(\mathbf{u} - \mathbf{u}_0) \quad (4)$$

The vectors  $\Delta \mathbf{x} = \mathbf{x} - \mathbf{x}_0$  and  $\Delta \mathbf{u} = \mathbf{u} - \mathbf{u}_0$  are known as respectively the incremental state vector and the incremental control input [27]. Due to the time separation principle [22], [27], [51], we can assume that the increment in the state  $\Delta \mathbf{x}$  is much smaller

than the increment in both the state derivative  $\Delta \dot{\mathbf{x}} = \dot{\mathbf{x}} - \dot{\mathbf{x}}_0$  and the input  $\Delta \mathbf{u}$ , and the dynamics (4) can be further simplified

$$\Delta \dot{\mathbf{x}} \cong \mathbf{B}_0 \Delta \mathbf{u} \quad (5)$$

where  $\mathbf{B}_0 = \frac{\partial \mathbf{f}_x(\mathbf{x}, \mathbf{u})}{\partial \mathbf{u}}$  is a control effectiveness matrix.

The dynamics equation (5) states that the ID of the system is produced by the control input increment. For the implementation of such a concept, it is assumed that the sampling time is small. In this case, the assumption that  $\Delta \mathbf{x} \ll \Delta \dot{\mathbf{x}}$  and  $\Delta \mathbf{x} \ll \Delta \mathbf{u}$  becomes possible for a real aircraft because the control surface deflections directly affect the angular accelerations, whereas the angular rates are only changed by integrating these angular accelerations. Actuators are assumed to be very fast, namely, the demanded input increment can be achieved within the small sampling time. In addition, it is assumed that the sensors are ideal, i.e. providing state derivative without errors.

#### 3.2. Attitude controller

The ID idea combined with the backstepping paradigm was utilized to design the aircraft baseline controller [49], [50]. Both angle and rate controllers were formulated using ID to increase the control robustness and simplify implementation. Fig. 1 shows the general structure of the baseline controller with the revealed interaction between attitude and rate controllers.

Eqs. (1) and (2) constitute the system dynamics. Introducing the kinematics tracking error variable  $\mathbf{z}_\xi = \xi_d - \xi$ , where  $\xi_d$  is the desired kinematics state vector, the sub-system (1) can be reformulated in terms of  $\mathbf{z}_\xi$ :

$$\dot{\mathbf{z}}_\xi = \dot{\xi}_d - \mathbf{f}_\xi - \mathbf{T}_\xi \boldsymbol{\omega} \quad (6)$$

The general idea behind the backstepping is to consider the state vector  $\boldsymbol{\omega} = [p \ q \ r]^T$  from (2) as a control input for  $\mathbf{z}_\xi$  subsystem (6). Since  $\boldsymbol{\omega}$  is just a state variable and not the real control input, it is called a virtual control input.

For the  $\mathbf{z}_\xi$  subsystem a Candidate Lyapunov Function (CLF)  $V_\xi$  is selected:

$$V_\xi = \frac{1}{2} \mathbf{z}_\xi^T \mathbf{z}_\xi, \quad (7)$$

which is positive for the whole domain, excluding the origin, where it equals to zero.

For the asymptotic convergence of the error, the CLF derivative must be strictly negative along the solutions of (6). Considering a positive definite matrix  $W_\xi \in \mathbb{R}^{3 \times 3}$ , the CLF is strictly negative if:

$$\dot{V}_\xi = \mathbf{z}_\xi^T \dot{\mathbf{z}}_\xi = -\mathbf{z}_\xi^T \mathbf{W}_\xi \mathbf{z}_\xi. \quad (8)$$

The kinematics tracking error dynamics can be represented in the incremental form

$$\dot{\mathbf{z}}_\xi = \dot{\xi}_d - \dot{\xi}_0 - \mathbf{T}_\xi (\boldsymbol{\omega} - \boldsymbol{\omega}_0). \quad (9)$$

Substituting the expression  $\dot{\mathbf{z}}_\xi = -\mathbf{W}_\xi \mathbf{z}_\xi$  derived from (8), the following tracking error dynamics is obtained

$$\dot{\xi}_d - \dot{\xi}_0 - \mathbf{T}_\xi (\boldsymbol{\omega} - \boldsymbol{\omega}_0) + \mathbf{W}_\xi \mathbf{z}_\xi = 0. \quad (10)$$

The virtual control law  $\mathbf{v}_\alpha = \boldsymbol{\omega}$  can be obtained by inversion of (10) with respect to  $\boldsymbol{\omega}$

$$\mathbf{v}_\alpha = \boldsymbol{\omega}_0 + \mathbf{T}_\xi^{-1} (\mathbf{W}_\xi \mathbf{z}_\xi + \dot{\xi}_d - \dot{\xi}_0), \quad (11)$$

since  $\mathbf{T}_\xi$  is invertible for the aircraft within the flight envelope. The control law (11) is used as a desired value for the virtual control input  $\boldsymbol{\omega}$ .

### 3.3. Rate controller

The difference between the dynamics of the state variable  $\mathbf{y} = [V_t \boldsymbol{\omega}^T]^T$  and its desired value  $\mathbf{y}_d = [V_{td} \boldsymbol{\omega}_d^T]^T$  is defined as the dynamics tracking error variable  $\mathbf{z}_y = \mathbf{y}_d - \mathbf{y}$ . It should be noted that the airspeed is introduced as a state to the dynamics state vector in order to design the controller that simultaneously tracks the airspeed and angular rates of the aircraft. To design a control law  $\mathbf{u}$  that ensures that  $\mathbf{z}_y$  converges to zero, the following CLF for the complete  $(\mathbf{z}_\xi, \mathbf{z}_y)$ -system is formed:

$$V_y = V_\xi + \frac{1}{2a} \mathbf{z}_y^T \mathbf{z}_y, \quad (12)$$

where  $a$  is the design scale factor. Similar to design of the CLF for the  $\mathbf{z}_\xi$  subsystem in (8), here the matrix  $\mathbf{W}_y \in \mathbb{R}^{4 \times 4}$  is assumed to be a positive definite matrix such that

$$\dot{V}_y = \dot{V}_\xi + \frac{1}{a} \mathbf{z}_y^T \dot{\mathbf{z}}_y = -\mathbf{z}_\xi^T \mathbf{W}_\xi \mathbf{z}_\xi - \frac{1}{a} \mathbf{z}_y^T \mathbf{W}_y \mathbf{z}_y. \quad (13)$$

Thus, the error  $\mathbf{z}_y$  converges asymptotically to zero since the derivative of the CLF  $V_y$  is strictly negative for non-zero errors. The tracking error dynamics in the incremental representation has the following form:

$$\dot{\mathbf{z}}_y = \dot{\mathbf{y}}_d - \dot{\mathbf{y}}_0 - \mathbf{B}_0 (\mathbf{u} - \mathbf{u}_0). \quad (14)$$

The selection matrix  $\mathbf{C}_{y\omega} = [\mathbf{0}_3 \quad \mathbf{I}_3]$ , which performs the mapping  $\boldsymbol{\omega} = \mathbf{C}_{y\omega} \mathbf{y}$ , is introduced. Combining the incremental dynamics of  $\mathbf{z}_\xi$  (9) and  $\mathbf{z}_y$  (14), one can obtain

$$\begin{aligned} \mathbf{z}_\xi^T (\dot{\xi}_d - \dot{\xi}_0 - \mathbf{T}_\xi (\mathbf{v}_\alpha - \mathbf{C}_{y\omega} \mathbf{z}_y - \boldsymbol{\omega}_0) + \mathbf{W}_\xi \mathbf{z}_\xi) \\ + \frac{1}{a} \mathbf{z}_y^T (\dot{\mathbf{y}}_d - \dot{\mathbf{y}}_0 - \mathbf{B}_0 (\mathbf{u} - \mathbf{u}_0) + \mathbf{W}_y \mathbf{z}_y) = 0. \end{aligned} \quad (15)$$

Eventually, for non-zero errors, substituting (11) into (15) and solving it with respect to  $\mathbf{u}$ , the resultant control law is designed

$$\mathbf{u}_c = \mathbf{u}_0 + \mathbf{B}_0^{-1} \boldsymbol{\Lambda} \left( a \mathbf{C}_{y\omega}^T \mathbf{T}_\xi^T \mathbf{z}_\xi + \mathbf{W}_y (\mathbf{y}_d - \mathbf{y}) + \dot{\mathbf{y}}_d - \dot{\mathbf{y}}_0 \right). \quad (16)$$

To attenuate the measurement noise and increase the control robustness,  $\mathbf{B}_0$  is multiplied by a diagonal matrix  $\boldsymbol{\Lambda} > 0$  with elements  $\lambda_{ii} \in [0, 1]$ .

The control law in the form (16) requires inversion of the matrix  $\mathbf{B}_0$ , which is not square for the overactuated modern transport aircraft. To tackle this issue, Moore-Penrose Pseudo-inverse (MPP) is applied [50], and

$$\mathbf{B}_0^\dagger = \mathbf{B}_0^T (\mathbf{B}_0 \mathbf{B}_0^T)^{-1} \quad (17)$$

is used in (16) instead of  $\mathbf{B}_0$ . MPP has satisfactory results if no singularities are expected in the system to be inverted [52].

The developed controller demonstrated excellent tracking performance, disturbance rejection, significant phase and gain margins [49], [50].

### 3.4. Command filter

To avoid infeasible commands provided by the controller, a Command Filter (CF) is added to the controller output. For the incremental controllers, the CF is used to constrain the input to respect the actuators dynamics and saturation.

Taking into account the influence of the CF  $\boldsymbol{\chi} \in \mathbb{R}^3$  on the tracking error  $\mathbf{z}_y$  (14) the dynamics of the modified tracking error  $\dot{\mathbf{z}}_y$  is introduced [27]

$$\dot{\mathbf{z}}_y = \dot{\mathbf{y}}_d - \dot{\mathbf{y}}_0 - \mathbf{B}_0 (\mathbf{u} - \mathbf{u}_0) - \dot{\boldsymbol{\chi}} \quad (18)$$

Effect of the CF on the tracking error can be estimated by the stable linear filter [27]:

$$\dot{\boldsymbol{\chi}} = -\mathbf{W}_y \boldsymbol{\chi} + \mathbf{B}_0 (\mathbf{u}_{CF} - \mathbf{u}_c), \quad (19)$$

where  $\mathbf{u}_{CF}$  is the controller output after CF.

## 4. On-line estimation of the model parameters

Finally, the cascaded baseline controller consists of attitude and rate controllers (11) and (16). Both attitude and rate controllers have a similar control structure, namely, the control signals compensating the difference between the reference and measured (or estimated) state variables are added to the current value of the control. Such a structure is very simple and robust to possible uncertainties. However, the precise knowledge of the relationship between the inner and outer loops  $\mathbf{T}_\xi$  and the control efficiency  $\mathbf{B}_0$  is required for the stable performance of the algorithm. Under normal circumstances, the precise value of  $\mathbf{T}_\xi$  within the flight envelope can be easily determined because it represents the kinematic relationship, however, failures in the measurement system can cause variations of this relationship. The matrix  $\mathbf{B}_0$  specifies the control effectiveness, which might change during flight because of changes in environmental conditions, structural deformations, failures etc. Hence, unmodeled actuator dynamics is a source of uncertainty.

The primary goal of the adaptive augmentation for the IBKS is to compensate for these uncertainties' effects and to improve the performance and stability of the IBKS controller. This paper introduces a general approach for indirect adaptation, compensating errors in  $\mathbf{T}_\xi$  and  $\mathbf{B}_0$ .

Let us first analyse the error in the system. In the considered case, the kinematics error is given with the following equation:

$$\dot{\mathbf{z}}_\xi = \boldsymbol{\Delta} \dot{\xi} - \mathbf{T}_\xi (\mathbf{w}_\xi) \boldsymbol{\Delta} \boldsymbol{\omega}, \quad (20)$$

where  $\mathbf{z}_\xi \in \mathbb{R}^{n_\xi}$ ,  $\boldsymbol{\Delta} \boldsymbol{\omega} \in \mathcal{X}_{\Delta\omega} \subseteq \mathbb{R}^{n_\omega}$ ,  $\boldsymbol{\Delta} \dot{\xi} \in \mathcal{X}_{\Delta\dot{\xi}} \subseteq \mathbb{R}^{n_\xi}$ , the nonlinear function  $\mathbf{T}_\xi : \mathbf{w}_\xi \mapsto \mathbb{R}^{n_\xi \times n_\omega}$  represents unknown kinematic relationship between angular rates and kinematic variables. Here  $\mathbf{w}_\xi = [\boldsymbol{\Delta} \dot{\xi}^T, \boldsymbol{\Delta} \boldsymbol{\omega}^T]^T$  is the concatenation introduced for the notation purposes. In a general case,  $\mathbf{T}_\xi$  is a function of increments of both angular rates and kinematic state derivatives. In a similar manner, notation  $\mathbf{W}_\xi = \mathcal{X}_{\Delta\omega} \times \mathcal{X}_{\Delta\dot{\xi}}$  is used to denote concatenations of subspaces of the state spaces.

The dynamics error is determined with the following equation

$$\dot{\mathbf{z}}_\omega = \boldsymbol{\Delta} \dot{\boldsymbol{\omega}} - \mathbf{B}_0 (\mathbf{w}_\omega) \boldsymbol{\Delta} \mathbf{u}, \quad (21)$$

where  $\mathbf{z}_\omega \in \mathbb{R}^{n_\omega}$ ,  $\Delta \mathbf{u} \in \mathcal{X}_{\Delta u} \subseteq \mathbb{R}^{n_u}$ , the nonlinear function  $\mathbf{B}_0 : \mathbf{w}_\omega \mapsto \mathbb{R}^{n_\omega \times n_u}$ , where  $\mathbf{w}_\omega = [\Delta \dot{\xi}^T, \Delta \omega^T, \Delta \dot{\omega}^T, \Delta \mathbf{u}^T]^T$ , represents unknown kinematic relationship between the control inputs and the dynamics states.  $\mathbf{W}_\omega = \mathcal{X}_{\Delta \dot{\xi}} \times \mathcal{X}_{\Delta \omega} \times \mathcal{X}_{\Delta \dot{\omega}} \times \mathcal{X}_{\Delta u}$  is used to denote concatenations of subspaces of the state spaces.

*Assumption 1:* Increments of angular rates and control inputs are bounded  $\Delta \mathbf{u}_g = [\Delta \omega^T, \Delta \mathbf{u}^T]^T \leq \Delta \bar{\mathbf{u}}_g$ .

Such an assumption is natural from a practical point of view.

To minimize tracking errors (20) and (21), the nonlinear functions  $\mathbf{T}_\xi$ ,  $\mathbf{B}_0$  should be identified. The identification problem is formulated as estimation of GP posterior means and covariances describing individual coefficient of  $\mathbf{T}_\xi$  and  $\mathbf{B}_0$

$$\begin{aligned} \hat{T}_{\xi_{i,j}} &\sim \mathcal{GP} \left( (T_{\xi_{i,j}}) \mathbf{K}_{T_{\xi_{i,j}}} \right) \quad i = 1 \dots n_\xi, j = 1 \dots n_\omega, \\ \hat{B}_{0_{i,j}} &\sim \mathcal{GP} \left( (B_{0_{i,j}}) \mathbf{K}_{B_{0_{i,j}}} \right) \quad i = 1 \dots n_\omega, j = 1 \dots n_u. \end{aligned} \quad (22)$$

## 5. Gaussian processes on-line identification and adaptive augmentation

GP utilizes the Bayesian paradigm for on-line identification of the model parameters and adaptive control by considering the identification as a statistical problem [41]. GP is non-parametric because the “parameters” to be identified are functions  $f_x$  of an input variable  $\mathbf{x} \in \mathbb{R}^d$ . Function  $f_x$  is characterised by its statistics, namely, by the mean  $\langle f_x \rangle$  and the covariance, which is also called the kernel  $\mathbf{K}_0(x, x') = \text{Cov}(\zeta, \zeta')$  [53]. The a priori assumption is that  $f_x$  is a Gaussian process. Indeed, according to the Central Limit Theorem, any sufficiently large set of random samples  $f_i$  is considered to have a normal distribution. Within the Bayesian framework, given a set of input-output observations  $(x_n, \zeta_n)$  ( $n = 1, \dots, N$ ) the posterior distribution of the process  $f_x$  is computed using prior and the likelihood.

Csató and Opper [41] proposed a representation of posterior means  $\langle f_x \rangle_t = \langle f(x_t) \rangle_t$  and the posterior covariance  $\mathbf{K}_t(x, x')$ , where  $t$  denotes the number of data points, with a finite linear combination of kernels  $\mathbf{K}_0(x, x_i)$  evaluated at the training inputs  $x_i$ . Using sequential projections of the posterior process on the manifold of Gaussian processes, approximate estimations of the representation effective parameters are obtained via recursions. To avoid enormous growth of the size of representations an elegant algorithm for extraction of a smaller subset of input data is proposed. Such a subset allows an on-line sparse representation of the posterior process, which is used to predict the GP model.

The posterior expectations within the Bayesian approach are conventionally expressed by high-dimensional integrals. This is not applicable for on-line identification. However, it was shown in [41] that the posterior mean and the posterior covariance of the process at arbitrary inputs can be expressed as a combination of a finite set of parameters which depend on the training data only. To make Bayesian interference trackable on-line the posterior is projected to the closest Gaussian process by a single sequential sweep through the examples.

The posterior GP approximation with its posterior means and the posterior covariance is estimated using the initial kernel  $\mathbf{K}_0(x, x')$  and the likelihoods:

$$\begin{aligned} \langle f_x \rangle_t &= \boldsymbol{\alpha}_t^T \mathbf{k}_x \\ \mathbf{K}_t(x, x') &= \mathbf{K}_0(x, x') + \mathbf{k}_x^T \mathbf{C}_t \mathbf{k}_{x'} \end{aligned} \quad (23)$$

where  $\mathbf{k}_x = [K_0(x_1, x), \dots, K_0(x_t, x)]^T$  is the kernel functions,  $\boldsymbol{\alpha}_t = [\alpha_t(1), \dots, \alpha_t(t)]^T$  is the coefficient,  $\mathbf{C}_t = \{C_t(ij)\}_{i,j=1 \dots t}$  is the coefficient matrix. It should be noted that coefficients  $\alpha_t(i)$  and  $C_t(ij)$  do not depend on  $x$  and  $x'$  [41]. For the regression problems, Radial Basis Functions (RBF) are quite popular choice for kernel functions

$$K(x, x') = \exp\left(-\frac{\|x - x'\|^2}{2\sigma_x^2}\right). \quad (24)$$

### 5.1. On-line learning

The recursive update of the GP parameters in Eq. (23) can be performed via the following equations:

$$\begin{aligned} \boldsymbol{\alpha}_{t+1} &= \mathbf{T}_{t+1}(\boldsymbol{\alpha}_t) + q^{(t+1)} \mathbf{s}_{t+1}, \\ \mathbf{C}_{t+1} &= \mathbf{U}_{t+1}(\mathbf{C}_t) + r^{(t+1)} \mathbf{s}_{t+1} \mathbf{s}_{t+1}^T, \\ \mathbf{s}_{t+1} &= \mathbf{T}_{t+1}(\mathbf{C}_t \mathbf{k}_{t+1}) + \mathbf{e}_{t+1}, \end{aligned} \quad (25)$$

where  $\mathbf{k}_{t+1} = \mathbf{k}_{x_{t+1}}$  and  $\mathbf{e}_{t+1}$  is the  $(t+1)$ -th unit vector, and  $\mathbf{s}_{t+1}$  is introduced for clarity. Operators  $\mathbf{T}_{t+1}$  and  $\mathbf{U}_{t+1}$  extend a  $t$ -dimensional vector and matrix to  $(t+1)$ -dimensional ones by appending zeros at the end of the vector and to the last row and column of the matrix respectively.

For the RBF kernel functions, the  $q^{(t+1)}$  and  $r^{(t+1)}$  are defined as follows

$$\begin{aligned} q^{(t+1)} &= (\zeta - \boldsymbol{\alpha}_t^T \mathbf{k}_x) / \sigma_x^2, \\ r^{(t+1)} &= -1 / \sigma_x^2, \end{aligned} \quad (26)$$

where  $\sigma_x^2 = \sigma_0^2 + \mathbf{k}_x^T \mathbf{C}_t \mathbf{k}_x + k_x^*$ ,  $k_x^* = K_0(x, x)$ . One can conclude that the dimension of the vector  $\boldsymbol{\alpha}$  and the size of matrix  $\mathbf{C}$  increases with each data point added since  $\mathbf{e}_{t+1}$  is the  $(t+1)$ -th unit vector.

The updates in the form of Eqs. (25) has a drawback since the number of parameters increases quadratically with the number of training examples. An effective way of controlling the number of parameters was proposed in [41], namely, sparseness within the GP framework was introduced. According to this approach, the update of the GP parameters is implemented without increase in the number of parameters  $\boldsymbol{\alpha}$  and  $\mathbf{C}$  when, according a certain criterion, the error due to the approximation is not too large.

If the new input  $x_{t+1}$  is such that

$$\mathbf{K}_0(x, x_{t+1}) = \sum_{i=1}^t \hat{\mathbf{e}}_{t+1}(i) K_0(x, x_i) \quad (27)$$

is true for all  $x$ , then the update can be achieved exactly. In this case, the updated process in the form of Eq. (23) is represented by only the first  $t$  inputs, but with “renormalised” parameters  $\hat{\boldsymbol{\alpha}}$  and  $\hat{\mathbf{C}}$  and update (25) is implemented without extending the size of the parameters  $\boldsymbol{\alpha}$  and  $\mathbf{C}$  and  $\mathbf{s}_{t+1}$  as follows:

$$\begin{aligned} \hat{\boldsymbol{\alpha}}_{t+1} &= \boldsymbol{\alpha}_t + q^{(t+1)} \hat{\mathbf{s}}_{t+1}, \\ \hat{\mathbf{C}}_t &= \mathbf{C}_t + r^{(t+1)} \hat{\mathbf{s}}_{t+1} \hat{\mathbf{s}}_{t+1}^T, \\ \hat{\mathbf{s}}_{t+1} &= \mathbf{C}_t \mathbf{k}_{t+1} + \hat{\mathbf{e}}_{t+1}, \end{aligned} \quad (28)$$

where  $\hat{\boldsymbol{\alpha}}_{t+1}$ ,  $\hat{\mathbf{C}}_t$  and  $\hat{\mathbf{s}}_{t+1}$  are  $t$ -th unit vectors.

Obviously, for most kernels and inputs  $x_{t+1}$  relationship (27) does not hold for all input  $x$ . However, the updates in the form of (28) might be used for approximations if  $\hat{\mathbf{e}}_{t+1}$  is determined by minimising the error measure

$$\left\| K_0(\cdot, x_{t+1}) - \sum_{i=1}^t \hat{\mathbf{e}}_{t+1}(i) K_0(\cdot, x_i) \right\|^2 \quad (29)$$

where  $\|\cdot\|$  is a norm in a space of functions of inputs  $x$ . If the norm is defined via the inner product of the reproducing kernel Hilbert space (RKHS) generated by the kernel  $K_0$ , then minimising (29), one can obtain the following expression

$$\hat{\mathbf{e}}_{t+1} = \mathbf{K}_t^{-1} \mathbf{k}_{t+1}, \quad (30)$$

where  $\mathbf{K}_t = \{K_0(x_i, x_j)\}_{i,j=1,t}$  is the Gram matrix. In this case, the equation

$$\hat{K}_0(x, x_{t+1}) = \sum_{i=1}^t \hat{e}_{t+1}(i) K_0(\cdot, x_i), \quad (31)$$

gives the orthogonal projection of the function  $K_0(x, x_{t+1})$  on the linear span of the functions  $K_0(x, x_i)$ .

The update rule (28) is performed when a measure of the approximation error

$$\gamma_{t+1} = k_{t+1}^* - \mathbf{k}_{t+1}^T \mathbf{K}_t^{-1} \mathbf{k}_{t+1} \quad (32)$$

does not exceed some tolerance level  $\epsilon_{\text{tol}} > 0$ . Here,  $k_{t+1}^* = K_0(x_{t+1}, x_{t+1})$ . Eq. (32) has a geometrical interpretation, namely, it is a square norm of the ‘‘residual vector’’ from the projection in the RKHS. Alternatively, it measures the ‘‘novelty’’ of the current input. If  $\gamma_{t+1}$  is higher than a threshold value, then the current input holds additional information as compared to the existing set of inputs, which is called a ‘‘basis vector set’’ or  $\mathcal{BV}$  set, and thus it should be added to this set. Proceeding sequentially, some of the inputs are left out and others are included in the  $\mathcal{BV}$  set. However, because of the projection (31), the inputs left out from the  $\mathcal{BV}$  set will still contribute to the final GP configuration – the one used for prediction and for measurement of the posterior uncertainties. But the latter inputs will not be stored and do not lead to an increase of the size in the parameter set [41].

To avoid computationally expensive inversion of the Gram matrix the recursive calculation of the inverse Gram matrix can be employed [41]:

$$\mathbf{Q}_{t+1} = \mathbf{Q}_t + \gamma^{-1} (\hat{\mathbf{e}}_{t+1} - \mathbf{e}_{t+1}) (\hat{\mathbf{e}}_{t+1} - \mathbf{e}_{t+1})^T, \quad (33)$$

where  $\mathbf{e}_{t+1}$  is the  $(t+1)$ -th unit vector. All matrix inversion is excluded using this recursion relationship. The Gram matrix is guaranteed to be non-singular since only inputs with novel information about Gaussian process are included in the  $\mathcal{BV}$  set and  $\gamma_{t+1} > 0$  guarantees non-singularity of the extended Gram matrix.

## 5.2. Deleting a basis vector

Recursive update of the GP parameters (25) is implemented while the  $\mathcal{BV}$  set does not exceed the budget, namely, the maximum number of elements in  $\mathcal{BV}$ . Thus, a pruning procedure is required. When a new example is estimated as novel, this procedure should get rid of one of the basis vectors and replace it by the new input vector. Two different strategies can be applied for selection of the vector from the  $\mathcal{BV}$  set. The first strategy supposed to add a novel input vector instead of the oldest basis vector [46]. The second strategy [41] proposes to replace the basis vector with the smallest error. The former might be preferred for a fast-varying process. However, here we will follow the later approach since it provides enhanced richness of the  $\mathcal{BV}$  set and an improved long-term memory.

The removal procedure assumes that the respective  $\mathcal{BV}$  was added and the previous update step (28) was implemented. In this case,  $\alpha_{t+1}$  has  $(t+1)$  elements, and  $\mathbf{C}_{t+1}$  and  $\mathbf{Q}_{t+1}$  are the  $(t+1) \times (t+1)$  matrices. If we assume that the last added element should be deleted the decomposition of the  $\alpha_{t+1}$ ,  $\mathbf{C}_{t+1}$  and  $\mathbf{Q}_{t+1}$  could be represented as follows:

$$\alpha_{t+1} = \begin{bmatrix} \alpha_t^l \\ \alpha^r \end{bmatrix}, \mathbf{C}_{t+1} = \begin{bmatrix} \mathbf{C}_t^l & \mathbf{c}^r \\ \mathbf{c}^{rT} & c^r \end{bmatrix}, \mathbf{Q}_{t+1} = \begin{bmatrix} \mathbf{Q}_t^l & \mathbf{q}^r \\ \mathbf{q}^{rT} & q^r \end{bmatrix}, \quad (34)$$

where  $\mathbf{C}_t^l$  and  $\mathbf{Q}_t^l$  are  $t \times t$  sub-matrices extracted from the  $(t+1) \times (t+1)$  matrices  $\mathbf{C}_{t+1}$  and  $\mathbf{Q}_{t+1}$ . For the sake of simplicity, this representation is shown for the case when the last element

should be removed, however, similar partitioning could be done for a general case. Updating equations for the element deleting case are the following:

$$\begin{aligned} \hat{\alpha} &= \alpha_t^l - \alpha^r \frac{\mathbf{q}^{rT}}{q^r}, \\ \hat{\mathbf{C}} &= \mathbf{C}_t^l + \mathbf{c}^r \frac{\mathbf{q}^{rT}}{q^r} - \frac{1}{q^r} [\mathbf{q}^r \mathbf{c}^{rT} + \mathbf{c}^r \mathbf{q}^{rT}], \\ \hat{\mathbf{Q}} &= \mathbf{Q}_t^l - \frac{\mathbf{q}^r \mathbf{q}^{rT}}{q^r}, \end{aligned} \quad (35)$$

where  $\hat{\alpha}$ ,  $\hat{\mathbf{C}}$  and  $\hat{\mathbf{Q}}$  are the parameters after the deletion of the last basis vector and  $\alpha_t^l$ ,  $\mathbf{C}_t^l$ ,  $\mathbf{Q}_t^l$ ,  $\alpha^r$ ,  $\mathbf{c}^r$ ,  $\mathbf{q}^r$ ,  $c^r$  and  $q^r$  are taken from GP parameters before deletion.

To decide the element of the  $\mathcal{BV}$  set to be deleted a measure of change on the sample averaged posterior mean of the GP due to the sparse approximation is used [41]. This leads to the following score measure for each element  $i$ :

$$\epsilon_i = \frac{|\alpha_{t+1}(i)|}{\mathbf{Q}_{t+1}(i, i)}. \quad (36)$$

The basis vector with minimal score (36) is deleted.

This method provides deleting of a basis vector from the  $\mathcal{BV}$  set with minimal loss of information.

Finally, the budgeted sparse GP algorithm is summarized by Algorithm 1.

---

### Algorithm 1 Budgeted sparse GP algorithm.

---

- 0: Initialize the  $\mathcal{BV}$  set with an empty set, maximum number of the set elements with  $d$ , a tolerance with  $\epsilon_{\text{tol}}$ ,  $\alpha$ ,  $\mathbf{C}$ ,  $\mathbf{Q}$  with empty values.  
 For each new measurement  $(x_{t+1}, \zeta_{t+1})$  **iterate**
1. Compute  $\mathbf{q}^{t+1}$ ,  $\mathbf{r}^{t+1}$ ,  $k_{t+1}^*$ ,  $\mathbf{k}_{t+1}$ ,  $\hat{\mathbf{e}}_{t+1}$  and  $\gamma_{t+1}$ .
  2. **If**  $\gamma_{t+1} < \epsilon_{\text{tol}}$  **then**  
 Perform a reduced update using (28).
  3. **else**  
 Perform an update using (25). Add the current input to the  $\mathcal{BV}$  set, and compute the inversed Gram matrix using (33).
  4. **If**  $|\mathcal{BV}| > d$  **then**  
 Compute scores for the  $\mathcal{BV}$  elements via (36) find the vector corresponding to the lowest score, and delete it using (35).
- 

## 5.3. Convergence analysis

In this section, the convergence of the GP adaptive IBKS closed-loop system is analysed.

After  $N$  measurements for each coefficient of matrices  $\mathbf{T}_\xi$  and  $\mathbf{B}_0$ , the maximum information gain is introduced with the following equation [54]

$$\gamma_{i,j}^N = \max_{\tilde{\mathbf{w}}_{i,j}^{(1)}, \dots, \tilde{\mathbf{w}}_{i,j}^{(N)} \in W_{i,j}} \frac{1}{2} \log \left| \mathbf{I} + \sigma_{i,j}^{-2} \tilde{\mathbf{K}}_{i,j} \right|, \quad (37)$$

where  $\left[ \tilde{\mathbf{K}} \right]_{ab} = k(\tilde{x}_{ij}^{(a)}, \tilde{x}_{ij}^{(b)})$  and  $|\cdot|$  is the determinant operator.

$\gamma_{i,j}^N$  can be interpreted as a measure of reduction of uncertainty achievable in a setting where the measurements are taken in the best possible fashion [54]. On a compact set  $W_{i,j}$ ,  $\gamma_{i,j}^N$  has a sublinear dependence on  $N$  for a multitude of kernels and can efficiently be approximated up to a small constant by utilizing the approach given in [55]. The following theorem from [56] gives estimates of the bound for the model error obtained when using a GP trained with noisy measurements.

**Theorem 1.** *Let  $f: W_{i,j} \rightarrow \mathbb{R}$  be a nonlinear function,  $B_f \in \mathbb{R}$  be a bound for the corresponding RKHS norm w.r.t.  $k_{ij}$ , i.e.,  $\|f\|_{k_{ij}} \leq B_f$ , and let  $\delta \in (0, 1)$ . For all  $N \in \mathbb{N}$ , define  $\beta_N = B_f + 4\sigma \sqrt{\gamma_{i,j}^N + 1 + \ln(\frac{1}{\delta})}$ , where  $\gamma_{i,j}^N$  is determined by (37). Then, for all  $N \geq 1$  and  $x_{ij} \in W_{i,j}$ , the following holds with probability of at least  $1 - \delta$*

$$|f(x_{ij}) - \langle f(x_{ij}) \rangle| \leq \beta_N \sigma_{N-1}(x_{ij}), \quad (38)$$

where  $N$  is a number of system measurements.

If  $B_f$  is not available a priori, a guess-and-doubling strategy can be employed to obtain an estimate,  $\sigma$  can be estimated by sampling the same data point multiple times [54], [55]. Since  $\gamma_{ij}^N$  grows sub-linearly with  $N$  on a compact set, the term  $\beta_N$  grows slowly with  $N$  on a compact set. The covariance term  $\sigma_{N-1}(x_{ij})$  typically is very small next to training data points [57]. Hence, the variance term  $\sigma_{N-1}(x_{ij})$  can be decreased if the region of interest is sampled densely enough. This is achieved on a compact set [54], [55] by selecting training data points  $x_{ij}$  corresponding to highest model uncertainty, i.e.,

$$x_{ij}^{(N+1)} = \arg \max_{x_{ij} \in \mathcal{X}_{ij}} \sigma_N(\tilde{x}_{ij}). \quad (39)$$

Following approach proposed in [45], we can state the next Lemma, showing that **Algorithm 1**, which utilizes a sparse GP representation, keeps error  $\epsilon_f = f(x_i) - \langle f(x_i) \rangle$  induced by the projection bounded.

**Lemma 1.** *Let the unknown function  $f$  be representable by a GP,  $\langle f_x \rangle_t$  be an on-line estimated GP representation of the function via a sparse subset  $\mathcal{B}\mathcal{V}$  of the data selected by deleting either the oldest basis vector or the basis vector with minimal score (36), then error  $\epsilon_f = f(x_i) - \langle f(x_i) \rangle$  is bounded with the probability of at least  $1 - \delta$ .*

**Proof.** According to [41] and the nonparametric Representer theorem [58] the sample averaged posterior mean of the GP has the following error due to the sparse approximation:

$$|\epsilon_{t+1}| = \frac{|f(x_i) - \langle f(x_i) \rangle|}{\sigma_x^2} \left| k_{t+1}^* - \mathbf{k}_{t+1}^T \mathbf{K}_t^{-1} \mathbf{k}_{t+1} \right|. \quad (40)$$

According to **Algorithm 1**  $\gamma_{t+1} = k_{t+1}^* - \mathbf{k}_{t+1}^T \mathbf{K}_t^{-1} \mathbf{k}_{t+1} < \epsilon_{\text{tol}}$ . Using Lemma 1 it could be derived that  $|f(x_i) - \langle f(x_i) \rangle| \leq \beta_N \sigma_{N-1}(x_i)$  due to (38). Thus, it can be concluded that  $|\epsilon_{t+1}| < \epsilon_{\text{tol}} \beta_N \sigma_{N-1}(x_i) / \sigma_x^2$  with probability of at least  $1 - \delta$ .  $\square$

Now the boundedness of the tracking error can now be proven.

**Lemma 2.** *Consider the tracking error given by (37) and the control law given with (16). The system tracking error  $\mathbf{z}_g = [\mathbf{z}_\xi^T \mathbf{z}_y^T]^T$  is globally uniformly ultimately bounded. With probability, of at least  $1 - \delta$ , the system ultimate error is given with*

$$\lim_{t \rightarrow \infty} |\mathbf{z}_g| = \sqrt{\sum_{i,j} \left( \frac{[\mathbf{W}_g^{-1}]_{ij} \beta_{ij}^T \sigma_{N-1ij} \epsilon_{\text{tol}ij} \Delta \bar{\mathbf{u}}_{gij}}{\sigma_{x_{ij}}^2} \right)^2}. \quad (41)$$

The Lyapunov function of the system given with Eq. (12) can be rewritten with the following

$$V \triangleq \frac{1}{2} \mathbf{z}_g^T \mathbf{z}_g, \quad (42)$$

where  $\mathbf{z}_g = [\mathbf{z}_\xi^T, \mathbf{z}_\omega^T / a]^T$ . For the brevity, let us designate  $\mathbf{B}_g = \begin{bmatrix} \mathbf{T}_\xi & 0 \\ 0 & \mathbf{B}_0 \end{bmatrix}$ , the estimation error is as follows  $\tilde{\mathbf{B}}_g = \mathbf{B}_g - \hat{\mathbf{B}}_g$ . In this case the derivative (13) can be rewritten

$$\dot{V} = -\frac{1}{2} \mathbf{z}_g^T \mathbf{W}_g \mathbf{z}_g + \mathbf{z}_g^T \tilde{\mathbf{B}}_g \Delta \mathbf{u}_g. \quad (43)$$

The derivative is negative if

$$|\mathbf{z}_g| > 2 \left| \mathbf{W}_g^{-1} \tilde{\mathbf{B}}_g \Delta \mathbf{u}_g \right|. \quad (44)$$

Due to the assumption  $|\Delta \mathbf{u}_g|$  is bounded. Therefore, the inequality holds true for  $|\mathbf{z}_g|$  large enough, which means that  $|\mathbf{z}_g|$  is globally uniformly ultimately bounded. Taking into account Lemma 1, we get the desired result.  $\square$

It should be noted that  $\sigma_{N-1ij}$  and  $\sigma_{x_{ij}}$  are different; the former is due to approximation after  $N$  measurements, however, the latter is because of the on-line approximation.

The proof shows that the ultimate error bound of the controlled system with GP adaptation can be made arbitrarily small with a high probability by increasing the control gains  $\mathbf{W}_g$ , by reducing the tolerance level  $\epsilon_{\text{tol}ij}$ , which leads to less "residual vector" from the projection in the RKHS, or by selecting data points such that the terms  $\beta_{ij}^T \sigma_{N-1ij}$  are reduced. The latter can be achieved by collecting new measurements at points of high uncertainty. This is particularly interesting in a case where the control input  $|\Delta \mathbf{u}_g|$  is constrained and high gains  $\mathbf{W}_g$  are not possible. At the same time, estimation error bound benefits from baseline control law, which is used to enforce compactness of the portion of the state space explored by the state trajectory. This in turn can be employed to guarantee sub-linear dependence of  $\gamma_{ij}^N$  on  $N$ , which enables the ultimate bound of  $|\mathbf{z}_g|$  to be efficiently reduced with new training data. Furthermore, in [59], it was shown that the linear independence of  $\mathcal{B}\mathcal{V}$  ensures that persistency of excitation in the state space is visible in RKHS. Since the proposed algorithm aims to enforce this independence subject to the tolerance  $\epsilon_{\text{tol}ij}$ , PE is never lost (ensuring  $\mathbf{K}_t$  is invertible).

## 6. Control effectiveness estimation and IBKS adaptation loop

Due to the limited capacity of a journal paper, GP online identification framework is validated with the estimation of the aircraft control derivatives contained in matrix  $\mathbf{B}_0$ . Interaction of the adaptive augmentation with the baseline controller is demonstrated in Fig. 1. The adaptive augmentation block performs in-direct adaptation by online estimation and adjustment of the control effectiveness matrix  $\mathbf{B}_0$ .

Within the proposed framework the control efficiency is approximated via GP, which is characterized with its mean  $\langle \mathbf{f}_x \rangle$  and covariance  $\mathbf{K}(\mathbf{x}, \mathbf{x}')$ . For smooth identification process the components of the input vector are normalized. The output observations are the instantaneous control efficiency values  $\zeta$  estimated from (5) by dividing the increment of state derivate  $\Delta \dot{\mathbf{x}}$ , by increment of control input  $\Delta \mathbf{u}$

$$\zeta_i = \frac{\Delta \dot{\mathbf{x}}}{\Delta \mathbf{u}}. \quad (45)$$

To avoid singularity of the estimation due to division in (45), we added additional check of the input data, namely,

$$\Delta \mathbf{u} > \epsilon_{\mathbf{u}_{\text{tol}}}. \quad (46)$$

Further, the estimated value of the control efficiency is supplied to the IBKS controller as a new value of a corresponding coefficient in  $\mathbf{B}_0$ .

Another issue of the in-flight control effectiveness estimation is that an aircraft flight control system sends the same signals for all individual control surfaces, making the individual signals proportional to each other and causing a high correlation between the individual signals. If all the input signal forms look the same, then any algorithm trying to assign values for the control effectiveness of individual control will fail, because it is impossible to determine which of the multiple inputs, moved in the same manner,

**Table 1**  
Considered failure scenarios.

No	Scenario description	Elevator			
		Inner Left	Inner Right	Outer Left	Outer Right
1	50% reduction of the control efficiency $C_{m_s}$	50% of $C_{m_s}$	Working	Failed before $t=0$	Failed before $t=0$
2	1 <sup>st</sup> order nonlinear dynamics	$F(s) = (2s + 1)^{-1}$	Working	Failed before $t=0$	Failed before $t=0$
3	2 <sup>nd</sup> order nonlinear dynamics	$F(s) = (2s^2 + s + 1)^{-1}$	Working	Failed before $t=0$	Failed before $t=0$

was responsible for changes in the aerodynamic forces and moments. Input forms that are completely decorrelated will give the most accurate control effectiveness estimates. Unfortunately, when a feedback control system is operating, desired input forms become distorted by the feedback control. To tackle this issue, we use a priori information through fixing the effectiveness of all but one of the correlated control surfaces to a priori values similar to [35].

Furthermore, while identifying the effectiveness of a certain control surface, the aircraft is demanded to perform manoeuvres with reduced coefficients in the allocation matrix  $\mathbf{W}_s \mathbf{D}_u$  for all control effectors responsible for this motion, except the coefficient relating to the control surface under study. In such a case, the control signal is split into two signals, the first one is for the control surface of which effectiveness is treated, while the second signal is for all other surfaces from the pool. Thus, the first signal is responsible for generating the required information for identification and the second one is used for guaranteeing the aircraft stability. Here we follow the approach from [24]

To estimate effectiveness of individual control effectors, individual contribution from each of the effector is taken in identification scheme (45). So, instead of  $\Delta \dot{x}$ , we used

$$\Delta \dot{x}^{\text{ind}} = \Delta \dot{x} - \mathbf{W}_s \mathbf{D}_u \hat{\mathbf{B}}_0 \Delta \mathbf{u}^{\text{sup}},$$

where  $\Delta \dot{x}$  is the derivative increment,  $\mathbf{D}_u$  is the allocation matrix,  $\mathbf{W}_s$  is the amplification matrix required to produce the supporting control signal  $\mathbf{u}^{\text{sup}}$ . Elements of  $\mathbf{W}_s$  specify how the individual actuator signals differ from the generic one. The terms  $-\mathbf{W}_s \mathbf{D}_u \hat{\mathbf{B}}_0 \Delta \mathbf{u}^{\text{sup}}$ , which are responsible for the subtraction of contribution from the supporting signal to the flight dynamics, are introduced in order to obtain the pure dynamics produced by the treated control surface. The predictor variable  $\Delta \mathbf{u}$  in (45) is based on the incremental signal for the control surface under study.

We compared the proposed GP augmentation for IBKS with other adaptive strategies based on Recursive Least Square with Exponential Forgetting and Tuning functions (both techniques are provided in the Appendix for reference).

## 7. Simulation results

In this section, a simulation study of the ability of the discussed algorithm to tackle the failures is considered.

A nonlinear model of the Boeing 747 aircraft, courteously provided by the consortium partner TU Munich, is used to validate the designed approach. This model is a variant of the GARTEUR RECOVER benchmark simulator [6]. The Boeing 747 is a large, transport aircraft with four wing-mounted engines. It has a length of approximately 70 meters, wingspan of 60 meters, and the maximum take-off weight is greater than 300 tons. The actuation of the Boeing 747 simulator corresponds to four ailerons, four elevators, two rudders, and four engines.

The nominal condition from which the simulation starts is a straight flight towards North with 340 knot of True Airspeed (TAS) and at an altitude of 5000 ft. The flight is developed under a low

turbulence condition defined by a 20-foot wind of 15 m/s in North direction and a turbulence intensity exceedance probability of 0.01.

The algorithm is validated in the longitudinal motion of the aircraft. It is assumed that uncertainties are in the effectiveness of the elevator to control pitch. Three different scenarios were considered. In the first scenario, a control efficiency of the one of the elevators was reduced by half. In the second and third scenarios, a nonlinear dynamics of the first or the second order in one of the actuators was added. The summary of the considered cases is provided in Table 1. Additional explanation is provided below in the corresponding subsections.

For the GP identification, we had  $x_i = \frac{V_i}{V_{\text{norm}}}$ , where the normalizing constant  $V_{\text{norm}} = 345$  knot guarantees that the corresponding RBF centres are close to the unity. To have a proper comparison with EF RLS, we had the similar selection of the output data, namely,  $\varsigma_i = \Delta \dot{y}_i^{\text{ind}} - \mathbf{W}_s \mathbf{D}_u \hat{\mathbf{B}}_0 \Delta \mathbf{u}^{\text{sup}}$ . The maximum number  $d$  of the  $\mathcal{BV}$  set was 3,  $\epsilon_{\text{tol}} = 1e-4$ ,  $\epsilon_{u,\text{tol}} = 1e-4$ ,  $\sigma_0^2 = 5e-9$ . To obtain the appropriate overlapping between neighbouring kernels the RBF width is specified as follows

$$\sigma = \frac{0.2}{4(\sqrt{d} - 1)^2}. \quad (47)$$

Forgetting function of EF RLS was  $F = 0.9999$ . Adaptation gain for the TF update law was  $\Gamma = 150$ .

### 7.1. Two failures and loss of effectiveness

In the current section an ability of the developed controller is evaluated in a case of simultaneous failure of two elevators (stuck-in-position) and 50% loss of effectiveness of the third elevator.

The results are presented in Fig. 2. Here it is assumed that two elevator failures (stuck-in-position) happened before  $t = 0$  s. For the adaptive algorithms, it is considered that these two failures detected and isolated also before  $t = 0$  s, which means that the corresponding coefficients equal to zero in the  $\hat{\mathbf{B}}_0$ . The loss of effectiveness of one of the two rest elevators, namely, Inner Left (IL), simulated at  $t = 5$  s.

On the top left subplot, estimation of the failed elevator effectiveness obtained with GP is demonstrated. One can see that the identification is finished within 230 s after the failure. At the same subplot, estimations provided by EF RLS and TF are also added for comparison purposes. One can see that the GP performance is pretty similar to EF RLS, however, TF is much slower. It should be mentioned, that the slow estimation rate exhibited by TF is due to the low adaptation gain and relatively small identification steps. They might be increased to improve the estimation rate, however, further increase of the rate/amplitude caused losses of the algorithm stability for other test cases. On the left bottom subplot, the pitch angle  $\theta$  is presented, while in the bottom right figure the pitch rate  $q$  is provided. On the right-top subplot the real effectiveness of two working elevators, namely, inner and outer elevators, are demonstrated. One can see that at  $t=5$  s the effectiveness of the inner elevator degraded (as assumed by the scenario). Effectiveness of the elevators failed before  $t=0$  s is zero.



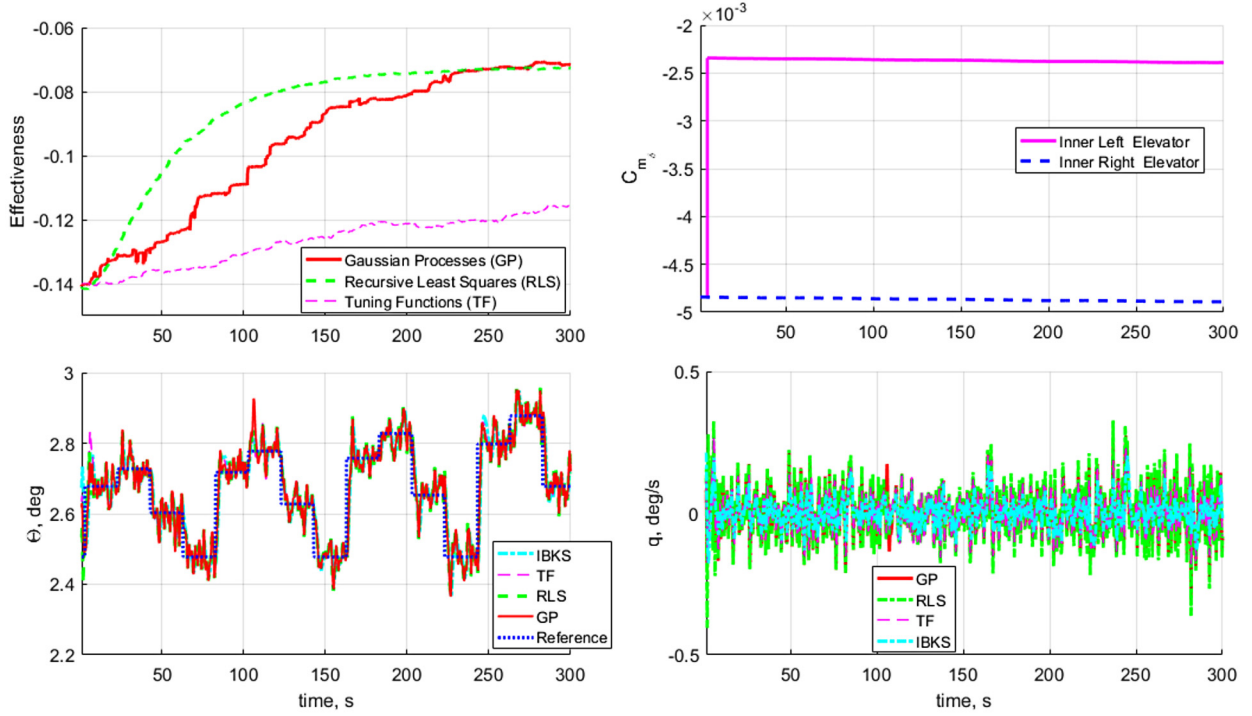


Fig. 2. First simulation scenario.

From the obtained results, one can conclude that the pure IBKS is quite robust to such types of failures, especially when actuation redundancy is available. When the mismatch between the real and model control efficiency is constant, i.e. when the system input affine property is conserved, the IBKS is able to cancel the produced uncertainty, which was also reported in [24], [29], [50]. Nevertheless, the online estimations of control effectiveness could improve the control quality. This example shows that the proposed online GP identification provides fast and precise tracking of the control effectiveness variation.

### 7.2. First order dynamics

Following the methodology proposed in [24], we also tested the ability of the algorithms to counteract the uncertainties when the system input affine property was broken. This section considers the appearance of the first-order unmodeled actuator dynamics.

A high level of redundancy (four elevators) allows for conserving the input affine property for Boeing 747, even in the case of the arising of unmodeled dynamics in one of the actuators. To simulate the conditions where the input affine property is not valid anymore, we assume here that two elevators failed before  $t = 0$  s. For the adaptive algorithms, similar to the previous scenario, it is considered that two elevator failures were detected and isolated before  $t = 0$  s and those corresponding coefficients equal to zero in  $\hat{\mathbf{B}}_0$ . Meanwhile, for the pure IBKS, it is considered, that the algorithm does not have access to new information about the control effectiveness and, thus, uses initial matrix  $\hat{\mathbf{B}}_0$ . At  $t = 150$  s, the nonlinear unmodeled dynamics originate at one of the two working actuators as a failure. It was reported that many known actuator failures could be simulated with the first or second order actuator dynamics [60], [61]. For the current scenario, we assumed the first order dynamics, represented with the following equation

$$F(s) = (2s + 1)^{-1}. \quad (48)$$

Comparison of behaviours of the GP-adaptive IBKS with other IBKS modification is presented in Fig. 3.

The top-level subplot demonstrates identification of the control effectiveness implemented with GP, EF RLS and TF techniques. The middle and bottom subplots show the parameters of the state vector  $\theta$  and  $q$ . The first-order actuator dynamics arose at  $t = 5$  s has a significant effect on the performance of the IBKS algorithm, namely, weakly damped oscillations are observed. Before  $t = 150$  s, the IBKS demonstrates robustness to the failures for small-amplitude steps; even with two failed elevators, it follows the reference signal. At the same time, for the moderate amplitude steps, one can observe weakly damped oscillations in  $\theta$  and  $q$ . These oscillations are heavily dumped when any of the adaptation augmentations is applied.

The figure demonstrates that GP identification is significantly faster than other methods and converges within 20 s. Such a fast adaptation leads to reduced overshoots in pitch and precise following the demanded signal. GP is capable of relatively fast adaptation as compared to the considered algorithms, even in the case of a small noise-to-signal ratio at  $t < 150$  s.

### 7.3. Second order dynamics

The IBKS performance degradation due to a loss of the input-affine property is shown in the previous section. In this simulation experiment, the condition is examined further, namely, the nonlinear dynamics of the second order in one of the actuators is injected. Similar to the previous test case, we also assume that two elevators failed before  $t = 0$  s; for the adaptive controller, it is considered that these two failures were detected and isolated before  $t = 0$  s, and those corresponding coefficients equal zero in  $\hat{\mathbf{B}}_0$ . At  $t = 150$  s at one of the rest actuators, the 2-nd order unmodeled dynamics arise as a result of the failure:

$$F(s) = (2s^2 + s + 1)^{-1}. \quad (49)$$

Shown in Fig. 4 is comparison between behaviour of IBKS and Adaptive IBKS in considered scenario.

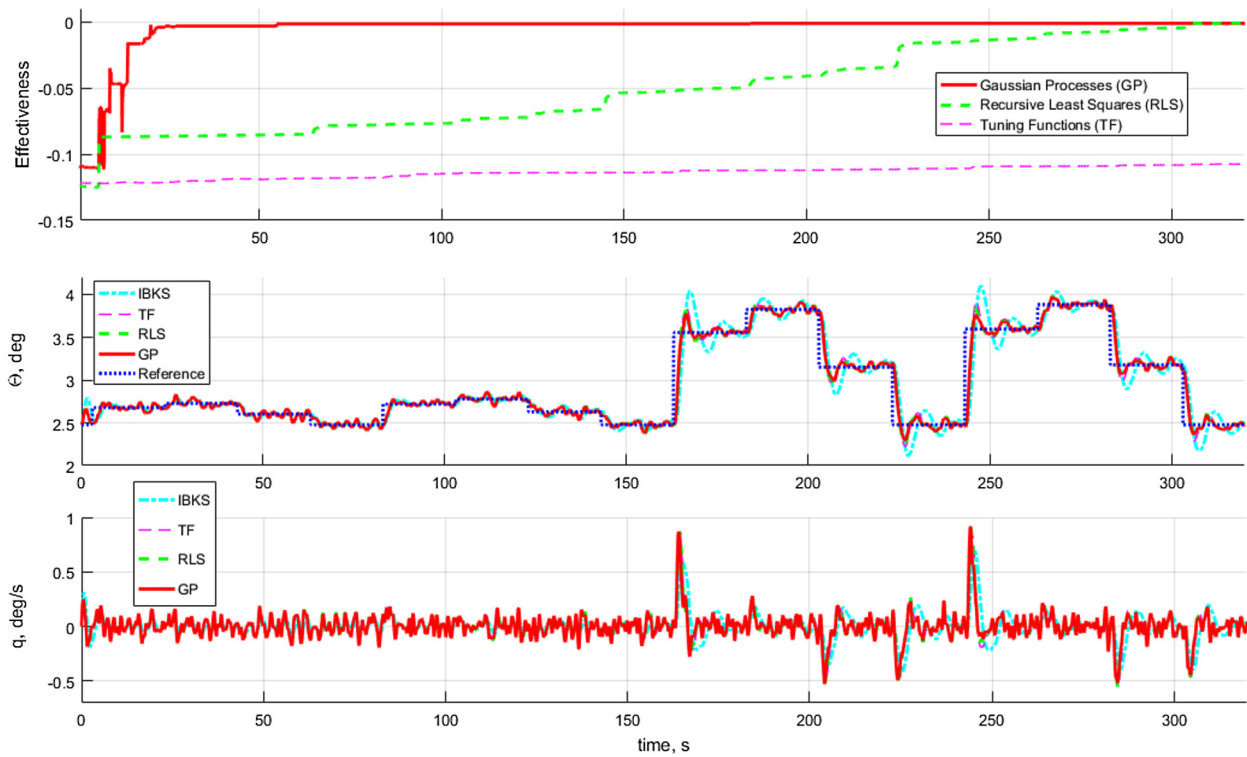


Fig. 3. 1<sup>st</sup> order nonlinear dynamics.

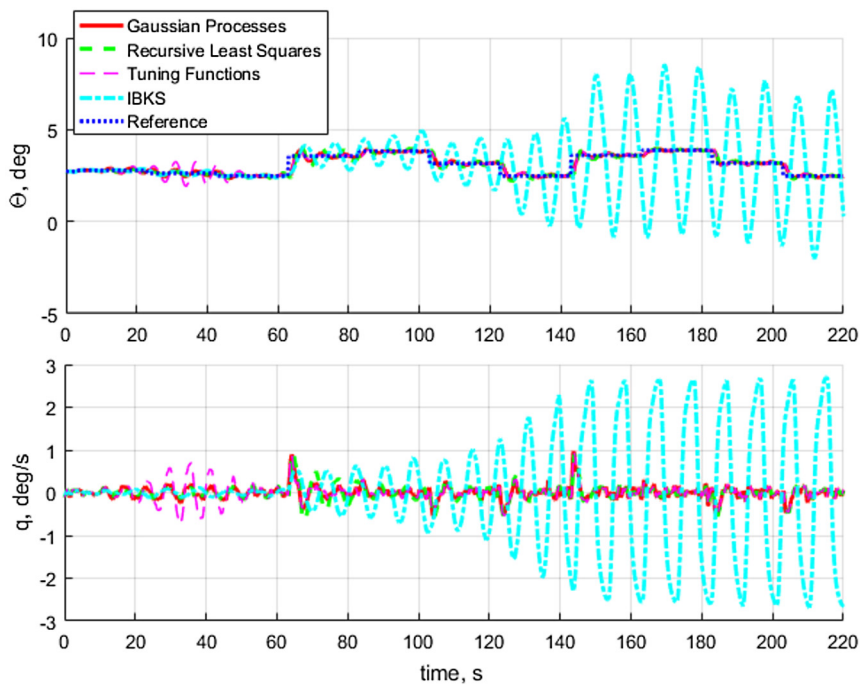


Fig. 4. 2<sup>nd</sup> order nonlinear dynamics.

Similar to the previous figures, the transition processes of state vector  $\theta$  and  $q$  are demonstrated. One can see that the IBKS control suffers from instability in the form of high-amplitude limit-cycle oscillations. Such a nonlinear dynamics is caused by interaction between the failed and the non-failed elevators. Meantime, IBKS with the adaptive augmentations manifests the system stability and good tracking performance.

Three different adaptive strategies are scrutinized in Fig. 5. All three algorithms provide stability. Similar to the previous sce-

nario, GP demonstrates the fastest adaptation rate and thus the best tracking performance among considered methods because it “switches off” harmful interaction of the failed and non-failed elevator.

**Remark 1.** The estimation convergence time is an important parameter of an adaptive system. The simulation results show that GP is doing better than other tested methods or the same in terms of convergence time. However, it might be noted that the time

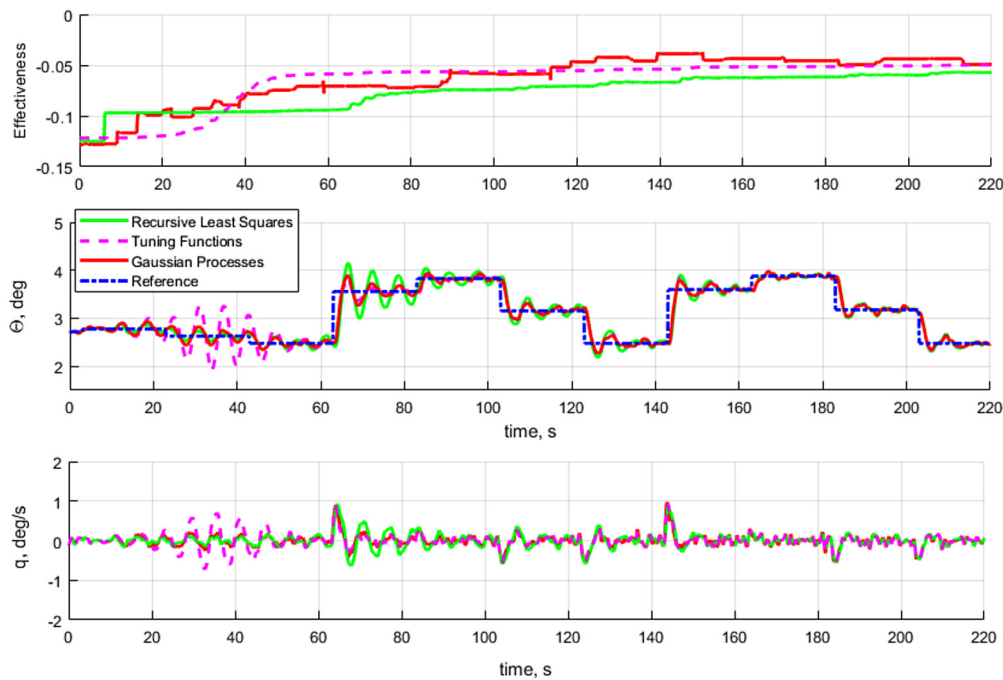


Fig. 5. Comparison of different estimators: 2<sup>nd</sup> order nonlinear dynamics.

is still large. Such large estimation times observed for all methods are because the estimations are performed for the closed-loop system, where the estimation algorithm interacts with the control system. Even though the convergence time varied from 20 seconds to 200 seconds, the augmented system remains stable, and the short-period dynamics is controlled even when the estimation is not converged.

**Remark 2.** Incremental Backstepping is a recently developed technique with a reduced dependency on the onboard aircraft model. This approach uses estimates of the state derivatives and the current actuator states to linearize the flight dynamics with respect to the current state. Our results and the results of the other researchers revealed the robustness of the IBKS to actuator failures when the system remains input affine, even in the case of multiple failures. However, we have shown in the current study that a combination of multiple failures and unmodelled actuator dynamics might cause a loss of input affine property. This property can also be lost in many other scenarios, for example, in the case of a combination of partial loss of effectiveness and transport delays. Furthermore, inaccurate measurements could introduce uncertainties in the matrix representing the relationship between the inner and outer loops. As a result, the system stability cannot be guaranteed anymore, and an adaptive augmentation is required to compensate the unmodelled dynamics.

**Remark 3.** Performance of the GP-adapted IBKS was studied in simulations of three different failure scenarios developed for Boeing 747 involving multiple failures with partial loss of effectiveness, and unmodelled actuator dynamics of the first and the second orders. The IBKS controller with model parameter estimator demonstrates improved stability and tracking performance characteristics. More precise information fed to the baseline controller by the estimator improved tracking performance for loss of effectiveness, cancelled undesired oscillations observed for the IBKS in case of unknown first-order actuator dynamics and prevented the loss of stability in case of unknown second-order actuator dynamics. The performance of the GP-adaptive IBKS is evaluated by comparison with EF RLS and TF. For the partial loss of efficiency, GP and

EF RLS demonstrated similar results. For the cases of unknown nonlinear actuator dynamics, GP showed faster adaptation leading to improved tracking performance. It is well known, that EF RLS works well, however, it shows less efficiency for time-varying processes. TF algorithm demonstrated slower adaptation because of the small adaptation gain; higher adaptation gains led to the loss of stability. Additional top-level algorithms, switching-on and switching-off TF-adaptation might be applied to make higher adaptation gains possible. However, such additional structures might make the overall control algorithm more complex. We could conclude that GP-based adaptation loop augmenting IBKS provides the best overall result among the considered methods.

## 8. Conclusions

In this research, we proposed a GP-based adaptive augmentation to IBKS, which uses the budgeted sparse GP algorithm for the online identification of the model parameters. The resulting tracking error is globally uniformly ultimately bounded, and its ultimate bound is decreased by increasing the control gains, reducing the tolerance to the error from the projection in the RKHS, or using additional training data.

Our results showed that IBKS with the model parameter estimator has improved stability and tracking performance characteristics and can guarantee the system stability under severe failures, even if the input-affine property is violated. GP-based adaptation overperforms other state-of-the-art methods, providing faster convergence and long-term memory. The resultant GP-adaptive IBKS control algorithm is almost model-free fault-tolerant control.

## Declaration of competing interest

The authors declare the following financial interests/personal relationships which may be considered as potential competing interests: Dmitry Ignatyev reports financial support was provided by European Union (INCEPTION project, which has received funding from the EU's Horizon2020 Research and Innovation Programme under grant agreement No. 723515).

## Data availability

The authors are unable or have chosen not to specify which data has been used.

## Acknowledgements

This research is partially funded by the European Union in the scope of INCEPTION project, which has received funding from the EU's Horizon2020 Research and Innovation Programme under grant agreement No. 723515.

## Appendix A. Adaptive augmentation for IBKS

We compared the proposed GP augmentation for IBKS with other adaptive strategies based on Recursive Least Square with exponential forgetting and Tuning functions.

### A.1. Recursive least square with exponential forgetting

The effectiveness is estimated online using the Recursive Least Square (RLS) with exponential forgetting (EF), which is commonly used for the real-time system identification. The technique enables recursive computations of estimates to be carried out. The typical algorithm for EF RLS is

$$\hat{\theta}(t) = \hat{\theta}(t-1) + \mathbf{P}(t)\boldsymbol{\varphi}(t) \left[ y(t) - \boldsymbol{\varphi}^T(t)\hat{\theta}(t-1) \right],$$

$$\mathbf{R}(t) = \mathbf{F}(t)\mathbf{R}(t-1) + \boldsymbol{\varphi}(t)\boldsymbol{\varphi}^T(t),$$

$$\mathbf{F} = \mu\mathbf{I}$$

where  $\hat{\theta}(t) \in R^n$  is the estimates of the parameter vector at time step  $t$ ,  $\boldsymbol{\varphi}(t) \in R^n$  is the observer data vector,  $y(t) \in R$  is the system output vector,  $\mathbf{P}(t) \in R^{n \times n}$  is the covariance matrix,  $\mathbf{R}(t) \in R^{n \times n}$  is the information matrix that is inverse of the covariance matrix,  $\mathbf{F}(t) \in R^{n \times n}$  is the forgetting matrix,  $\mu \in (0, 1)$  is the scalar forgetting factor.

The identification problem is stated as follows:

$$\zeta \cong \mathbf{A} \hat{\theta},$$

where the response variable vector is the following

$$\zeta = \left[ \Delta \dot{\mathbf{y}}_m^{\text{ind}}(1) - \mathbf{W}_s \mathbf{D}_u \hat{\mathbf{B}}_0 \Delta \mathbf{u}^{\text{sup}} \dots \Delta \dot{\mathbf{y}}_m^{\text{ind}}(N) - \mathbf{W}_s \mathbf{D}_u \hat{\mathbf{B}}_0 \Delta \mathbf{u}^{\text{sup}} \right]$$

$\Delta \dot{\mathbf{y}}_m^{\text{ind}}(1) \dots \Delta \dot{\mathbf{y}}_m^{\text{ind}}(N)$  is the record of derivative increment for  $m$  component of the dynamic state vector  $\mathbf{y}$ , the predictor variable vector is based on the incremental signal for the control surface under study

$$\mathbf{A} = \left[ \Delta \mathbf{u}^{\text{ind}}(1) \quad \Delta \mathbf{u}^{\text{ind}}(2) \dots \Delta \mathbf{u}^{\text{ind}}(N) \right]^T.$$

### A.2. Tuning functions

In the current section, we would like to present an adaptive augmentation to the baseline IBKS controller via the tuning function (TF) approach [16].

Here, we assume that actuator failure causes degradation of the actuation effectiveness. The dynamics of the general tracking error dynamics  $\mathbf{z}_g = \left[ \mathbf{z}_\xi^T \quad \mathbf{z}_y^T \right]^T \in R^7$ , which is measurable system state, is introduced with the following equations

$$\begin{aligned} \dot{\mathbf{z}}_\xi &= \dot{\xi}_d(t) - \dot{\xi}_0(\mathbf{z}_g, t) - \mathbf{T}_\xi(\boldsymbol{\omega}(\mathbf{z}_g, t) - \boldsymbol{\omega}_0(\mathbf{z}_g, t)), \\ \dot{\mathbf{z}}_y &= \dot{\mathbf{y}}_d(\boldsymbol{\omega}_0, t) - \dot{\mathbf{y}}(\mathbf{z}_g, t) - \mathbf{B}_0(t)(\mathbf{u}(\mathbf{z}_g, t) - \mathbf{u}_0(\mathbf{z}_g, t)) \\ &\quad - \dot{\chi}(\mathbf{u}, t), \end{aligned}$$

where  $\dot{\xi}_d, \dot{\xi}_0, \dot{\mathbf{y}}, \dot{\mathbf{y}}_d$  are essentially locally bounded, uniformly in  $t$  functions,  $\mathbf{B}_0(t)$  is the effectiveness matrix, an unknown, linear-parameterizable, essentially locally bounded function,  $\dot{\chi}$  is the influence of the CF, essentially locally bounded function,  $\mathbf{u}$  is the baseline control input.  $\hat{\mathbf{B}}_0: \mathbb{R}^{4 \times 14} \times (0, \infty) \rightarrow \mathbb{R}^{4 \times 14}$  is the estimate of  $\mathbf{B}_0$ . We assume that there exists an unknown parameter vector  $\hat{\theta} \in \mathbb{R}^k$  to be estimated such that  $j$ -column  $\hat{\mathbf{b}}_j \in \mathbb{R}^k$  of  $\hat{\mathbf{B}}_0^T$  can be represented as

$$\hat{\mathbf{b}}_j = \Phi_j^T(\xi_0, \mathbf{y}_0, \mathbf{u}_0, t)\hat{\theta},$$

where  $\Phi_j^T(\xi_0, \mathbf{y}_0, \mathbf{u}_0, t): \mathbb{R}^{3 \times 4 \times 14} \times (0, \infty) \rightarrow \mathbb{R}^{4 \times k}$  is the regressor function.

The estimation error is

$$\tilde{\mathbf{B}}_0 = \mathbf{B}_0 - \hat{\mathbf{B}}_0.$$

In this case, the parameter estimation errors and its derivative are the following

$$\tilde{\theta} = \theta - \hat{\theta}, \quad \dot{\tilde{\theta}} = -\dot{\hat{\theta}}.$$

For such a system, Lyapunov-based estimation algorithm can be designed

$$\dot{\hat{\theta}} = -\Gamma \Phi_j^T(\mathbf{x}_0, \mathbf{u}_0) \tilde{\mathbf{z}}_y \Delta \mathbf{u}_j,$$

where  $\Gamma \in \mathbb{R}^+$  are positive adaptation gains,  $\Delta \mathbf{u}_j$  is  $j$ th element of  $\Delta \mathbf{u}$ . Proof of stability could be found in [24], [27].

## References

- [1] EASA, European Aviation Safety Agency. Annual Safety Review 2014, 2014.
- [2] N.B. Abramov, M.G. Goman, A.N. Khrabrov, B.I. Soemarwoto, Aerodynamic modeling for poststall flight simulation of a transport airplane, *J. Aircr.* 56 (4) (2019) 1427–1440, <https://doi.org/10.2514/1.c034790>.
- [3] D.I. Ignatyev, M.E. Sidoryuk, K.A. Kolinko, A.N. Khrabrov, Dynamic rig for validation of control algorithms at high angles of attack, *J. Aircr.* 54 (5) (2017) 1760–1771, <https://doi.org/10.2514/1.c034167>.
- [4] D. Ignatyev, A. Khrabrov, Experimental study and neural network modeling of aerodynamic characteristics of canard aircraft at high angles of attack, *Aerospace* 5 (1) (2018) 26, <https://doi.org/10.3390/aerospace5010026>.
- [5] M.G. Goman, A.v. Khrantsovsky, E.N. Kolesnikov, Evaluation of aircraft performance and maneuverability by computation of attainable equilibrium sets, *J. Guid. Control Dyn.* 31 (2) (2008) 329–339, <https://doi.org/10.2514/1.29336>.
- [6] H. Smaili, B. Jan, T. Lombaerts, O. Stroosma, A benchmark for fault tolerant flight control evaluation, *IFAC Proc. Vol. (IFAC-PapersOnline)* (2009) 241–246, <https://doi.org/10.3182/20090630-4-ES-2003.0246>.
- [7] D.I. Ignatyev, A.N. Khrabrov, Neural network modeling of unsteady aerodynamic characteristics at high angles of attack, *Aerosp. Sci. Technol.* 41 (2015) 106–115, <https://doi.org/10.1016/j.ast.2014.12.017>.
- [8] D.I. Ignatyev, A.N. Khrabrov, A.I. Kortukova, D.A. Alieva, M.E. Sidoryuk, S.G. Bazhenov, Interplay of unsteady aerodynamics and flight dynamics of transport aircraft in icing conditions, *Aerosp. Sci. Technol.* 104 (2020) 105914, <https://doi.org/10.1016/j.ast.2020.105914>.
- [9] T. Yucelen, A.J. Calise, Derivative-free model reference adaptive control, *J. Guid. Control Dyn.* 34 (4) (2012) 933–950, <https://doi.org/10.2514/1.53234>.
- [10] N. Hovakimyan, C. Cao, L1 adaptive control theory: guaranteed robustness with fast adaptation 34 (4) (2010), <https://doi.org/10.2514/1.54082>.
- [11] Q.P. Chu, D.A. Joosten, M.H. Smaili, O. Stroosma, T.J.J. Lombaerts, J.A. Mulder, Piloted simulator evaluation results of new fault-tolerant flight control algorithm, *J. Guid. Control Dyn.* 32 (6) (2009) 1747–1765, <https://doi.org/10.2514/1.44280>.
- [12] G.P. Falconi, C.D. Heise, F. Holzapfel, Novel stability analysis of direct MRAC with redundant inputs, in: 24th Mediterranean Conference on Control and Automation, MED 2016, 2016, pp. 176–181.
- [13] J.H. Blakelock, *Automatic Control of Aircraft and Missiles*, 2nd ed., Wiley, New York, 1991.
- [14] S.P. Shue, M.E. Sawan, K. Rokhsaz, Mixed H/H8 method suitable for gain scheduled aircraft control, *J. Guid. Control Dyn.* 20 (4) (1997) 699–706, <https://doi.org/10.2514/2.4100>.
- [15] J.-J.E. Slotine, W. Li, *Applied nonlinear control* 62 (7) (1991), <https://doi.org/10.1366/000370208784909643>.
- [16] M. Krstic, P.v. Kokotovic, I. Kanellakopoulos, *Nonlinear and Adaptive Control Design*, 1st. ed, John Wiley & Sons, Inc., USA, 1995.

- [17] C.-H. Lee, T.-H. Kim, M.-J. Tahk, Agile missile autopilot design using nonlinear backstepping control with time-delay adaptation, *Trans. Jpn. Soc. Aeronaut. Space Sci.* 57 (1) (2014) 9–20.
- [18] J.R. Azinheira, A. Moutinho, E.C. de Paiva, Airship hover stabilization using a backstepping control approach, *J. Guid. Control Dyn.* 29 (4) (2006) 903–914, <https://doi.org/10.2514/1.17334>.
- [19] A. Tsourdos, B.A. White, Adaptive flight control design for nonlinear missile, *Control Eng. Pract.* 13 (3) (2005) 373–382, <https://doi.org/10.1016/j.conengprac.2004.04.023>.
- [20] P. Singh, D.K. Giri, A.K. Ghosh, Robust backstepping sliding mode aircraft attitude and altitude control based on adaptive neural network using symmetric BLF, *Aerosp. Sci. Technol.* 126 (2022) 107653, <https://doi.org/10.1016/j.ast.2022.107653>.
- [21] L.G. Sun, C.C. de Visser, Q.P. Chu, W. Falkena, Hybrid sensor-based backstepping control approach with its application to fault-tolerant flight control, *J. Guid. Control Dyn.* 37 (1) (2013) 59–71, <https://doi.org/10.2514/1.61890>.
- [22] S. Sieberling, Q.P. Chu, J.A. Mulder, Robust flight control using incremental nonlinear dynamic inversion and angular acceleration prediction, *J. Guid. Control Dyn.* 33 (6) (2010) 1732–1742, <https://doi.org/10.2514/1.49978>.
- [23] X. Wang, E.-J. van Kampen, Q. Chu, Quadrotor fault-tolerant incremental nonsingular terminal sliding mode control, *Aerosp. Sci. Technol.* 95 (2019) 105514, <https://doi.org/10.1016/j.ast.2019.105514>.
- [24] D.I. Ignatyev, H.S. Shin, A. Tsourdos, Two-layer adaptive augmentation for incremental backstepping flight control of transport aircraft in uncertain conditions, *Aerosp. Sci. Technol.* 105 (2020) 106051, <https://doi.org/10.1016/j.ast.2020.106051>.
- [25] P. Bhardwaj, V.S. Akkinapalli, J. Zhang, S. Saboo, F. Holzapfel, Adaptive augmentation of incremental nonlinear dynamic inversion controller for an extended f-16 model, *AIAA 2019-1923*, <https://doi.org/10.2514/6.2019-1923>, 2019, pp. 1–21.
- [26] B.-J. Jeon, M.-G. Seo, H.-S. Shin, A. Tsourdos, Understandings of incremental backstepping controller considering measurement delay with model uncertainty, *Aerosp. Sci. Technol.* 109 (2021) 106408, <https://doi.org/10.1016/j.ast.2020.106408>.
- [27] P. van Gils, E.-J. van Kampen, C.C. de Visser, Q.P. Chu, Adaptive incremental backstepping flight control for a high-performance aircraft with uncertainties, *AIAA 2016-1380*, <https://doi.org/10.2514/6.2016-1380>, 2016.
- [28] G.P. Falconi, V.A. Marvakov, F. Holzapfel, Fault tolerant control for a hexarotor system using incremental backstepping, in: *2016 IEEE Conference on Control Applications, CCA 2016*, vol. 1, 2016, pp. 237–242.
- [29] B.-J. Jeon, M.-G. Seo, H.-S. Shin, A. Tsourdos, Understandings of classical and incremental backstepping controllers with model uncertainties, *IEEE Trans. Aerosp. Electron. Syst.* 9251 (c) (2019) 1, <https://doi.org/10.1109/taes.2019.2952631>.
- [30] V.S. Akkinapalli, G.P. Falconi, F. Holzapfel, Fault tolerant incremental attitude control using online parameter estimation for a multicopter system, in: *2017 25th Mediterranean Conference on Control and Automation, MED 2017*, 2017, pp. 454–460.
- [31] D.I. Ignatyev, H.S. Shin, A. Tsourdos, Two-layer on-line parameter estimation for adaptive incremental backstepping flight control for a transport aircraft in uncertain conditions, *IFAC-PapersOnLine* 52 (12) (2019) 411–416, <https://doi.org/10.1016/j.ifacol.2019.11.278>.
- [32] D. Ignatyev, H.-S. Shin, A. Tsourdos, Two-layer fault detection for incremental flight control of fixed-wing UAV, in: *2019 Workshop on Research, Education and Development of Unmanned Aerial Systems (RED UAS)*, 2019, pp. 227–236.
- [33] D.I. Ignatyev, H.-S. Shin, A. Tsourdos, Fault detection, isolation and adaptive augmentation for incremental backstepping flight control, *IFAC-PapersOnLine* 53 (2) (2020) 14799–14804, <https://doi.org/10.1016/j.ifacol.2020.12.1912>.
- [34] B.W. Karl, Johan Åström, *Adaptive Control*, 2nd ed., Addison-Wesley Longman Publishing Co., Inc., Boston, MA, USA, 1994.
- [35] V. Klein, E. Morelli, *Aircraft System Identification - Theory and Practice*, AIAA, Blacksburg, USA, 2006.
- [36] H.-S. Shin, H.-I. Lee, A new exponential forgetting algorithm for recursive least-squares parameter estimation, <https://doi.org/10.48550/arXiv.2004.03910>, 2020.
- [37] A. Calise, Y. Shin, M. Johnson, A comparison study of classical and neural network based adaptive control of wing rock, <https://doi.org/10.2514/6.2004-5320>, 2004, pp. 1–17.
- [38] D.I. Ignatyev, H.S. Shin, A. Tsourdos, Bayesian calibration for multiple source regression model, *Neurocomputing* 318 (2018) 55–64, <https://doi.org/10.1016/j.neucom.2018.08.027>.
- [39] N. Boëly, R.M. Botez, New approach for the identification and validation of a nonlinear F/A-18 model by use of neural networks, *IEEE Trans. Neural Netw.* 21 (11) (2010) 1759–1765, <https://doi.org/10.1109/TNN.2010.2071398>.
- [40] K.S. Narendra, *Neural networks for control: theory and practice*, *Proc. IEEE* 84 (10) (1996) 1385–1406, <https://doi.org/10.1109/5.537106>.
- [41] L. Csató, M. Opper, Sparse on-line Gaussian processes, *Neural Comput.* 14 (3) (2002) 641–668, <https://doi.org/10.1162/089976602317250933>.
- [42] D. Ignatyev, H.-S. Shin, A. Tsourdos, Gaussian process adaptive incremental backstepping flight control, *AIAA 2022-2032*, <https://doi.org/10.2514/6.2022-2032>, 2022.
- [43] P.A. Ioannou, P.V. Kokotovic, Instability analysis and improvement of robustness of adaptive control, *Automatica* 20 (5) (1984) 583–594, [https://doi.org/10.1016/0005-1098\(84\)90009-8](https://doi.org/10.1016/0005-1098(84)90009-8).
- [44] B.W. Karl, Johan Åström, *Adaptive Control*, 2nd ed., Addison-Wesley Longman Publishing Co., Inc., Boston, MA, USA, 1994.
- [45] G. Chowdhary, H.A. Kingravi, J.P. How, P.A. Vela, Bayesian nonparametric adaptive control using Gaussian processes, *IEEE Trans. Neural Netw. Learn. Syst.* 26 (3) (2015) 537–550, <https://doi.org/10.1109/TNNLS.2014.2319052>.
- [46] R.C. Grande, G. Chowdhary, J.P. How, Experimental validation of Bayesian nonparametric adaptive control using Gaussian processes, *J. Aerosp. Inform. Syst.* 11 (9) (2014) 565–578, <https://doi.org/10.2514/1.i010190>.
- [47] <https://inception-h2020.tekever.com/>.
- [48] A. Varga, A. Hansson, G. Puyou, *Optimization Based Clearance of Flight Control Laws*, Springer, Berlin, Heidelberg, 2012.
- [49] R.A. Cordeiro, R. Azinheira, A. Moutinho, Cascaded incremental backstepping controller for the attitude tracking of fixed-wing aircraft, in: *5th CEAS Conference on Guidance, Navigation and Control*, 2019.
- [50] R.A. Cordeiro, J.R. Azinheira, A. Moutinho, Addressing actuation redundancies in incremental controllers for attitude tracking of fixed-wing aircraft, *IFAC-PapersOnLine* 52 (12) (2019) 417–422, <https://doi.org/10.1016/j.ifacol.2019.11.279>.
- [51] A.B. Paul, W. van Ekeren, Q.P. Chu, PI(D) tuning for flight control systems via incremental nonlinear dynamic inversion, *IFAC-PapersOnLine* 50 (1) (2017) 8175–8180, <https://doi.org/10.1016/j.ifacol.2017.08.1265>.
- [52] H. Evain, M. Rognant, D. Alazard, J. Mignot, Nonlinear dynamic inversion for redundant systems using the EKF formalism, in: *2016 American Control Conference (ACC)*, 2016, pp. 348–353.
- [53] V.N. Vapnik, *The Nature of Statistical Learning Theory*, second, Springer, 1999.
- [54] A. Capone, S. Hirche, Backstepping for partially unknown nonlinear systems using Gaussian processes, *IEEE Control Syst. Lett.* 3 (2) (2019) 416–421, <https://doi.org/10.1109/LCSYS.2018.2890467>.
- [55] N. Srinivas, A. Krause, S.M. Kakade, M.W. Seeger, Information-theoretic regret bounds for Gaussian process optimization in the bandit setting, *IEEE Trans. Inf. Theory* 58 (5) (2012) 3250–3265, <https://doi.org/10.1109/TIT.2011.2182033>.
- [56] S.R. Chowdhury, A. Gopalan, On kernelized multi-armed bandits, in: *Proceedings of the 34th International Conference on Machine Learning (PMLR)*, vol. 70, 2017, pp. 844–853.
- [57] C.E. Rasmussen, C.K.I. Williams, *Gaussian Processes for Machine Learning*, The MIT Press, 2005.
- [58] B. Schölkopf, R. Herbrich, A.J. Smola, *A Generalized Representer Theorem*, *Lecture Notes in Computer Science*, vol. 2111, 2001, pp. 416–426 (including subseries *Lecture Notes in Artificial Intelligence* and *Lecture Notes in Bioinformatics*).
- [59] H.A. Kingravi, G. Chowdhary, P.A. Vela, E.N. Johnson, Reproducing kernel Hilbert space approach for the online update of radial bases in neuro-adaptive control, *IEEE Trans. Neural Netw. Learn. Syst.* 23 (7) (2012) 1130–1141, <https://doi.org/10.1109/TNNLS.2012.2198889>.
- [60] J.D. Bošković, R.K. Mehra, Failure detection, identification and reconfiguration system for a redundant actuator assembly, *IFAC Proc. Vol. (IFAC-PapersOnline)* 36 (5) (2003) 411–416, [https://doi.org/10.1016/S1474-6670\(17\)36526-6](https://doi.org/10.1016/S1474-6670(17)36526-6).
- [61] J.D. Bošković, S.E. Bergstrom, R.K. Mehra, Adaptive accommodation of failures in second-order flight control actuators with measurable rates, in: *Proceedings of the American Control Conference*, vol. 2, 2005, pp. 1033–1038.

2023-02-28

# Sparse online Gaussian process adaptation for incremental backstepping flight control

Ignatyev, Dmitry I.

Elsevier

---

Ignatyev DI, Shin H-S, Tsourdos A. (2023) Sparse online Gaussian process adaptation for incremental backstepping flight control. *Aerospace Science and Technology*, Volume 136, May 2023, Article number 108157

<https://doi.org/10.1016/j.ast.2023.108157>

*Downloaded from Cranfield Library Services E-Repository*